energies

MDPI

*Article*

# Development and Experimental Validation of an Adaptive, Piston-Damage-Based Combustion Control System for SI Engines: Part 1—Evaluating Open-Loop Chain Performance

**Alessandro Brusa [1,*], Nicolò Cavina [1], Nahuel Rojo [1], Jacopo Mecagni [1], Enrico Corti [1], Vittorio Ravaglioli [1], Matteo Cucchi [2] and Nicola Silvestri [2]**

[1] Department of Industrial Engineering, School of Engineering and Architecture, University of Bologna, 40126 Bologna, Italy; nicolo.cavina@unibo.it (N.C.); nahuel.rojo2@unibo.it (N.R.); jacopo.mecagni2@unibo.it (J.M.); enrico.corti2@unibo.it (E.C.); vittorio.ravaglioli2@unibo.it (V.R.)

[2] Ferrari S.p.A., 41053 Maranello, MO, Italy; Matteo.Cucchi@ferrari.com (M.C.); Nicola.Silvestri@ferrari.com (N.S.)

* Correspondence: alessandro.brusa6@unibo.it

**Abstract:** This work is focused on the development and validation of a spark advance controller, based on a piston "damage" model and a predictive knock model. The algorithm represents an integrated and innovative way to manage both the knock intensity and combustion phase. It is characterized by a model-based open-loop algorithm with the capability of calculating with high accuracy the spark timing that achieves the desired piston damage in a certain period, for knock-limited engine operating conditions. Otherwise, it targets the maximum efficiency combustion phase. Such controller is primarily thought to be utilized under conditions in which feedback is not needed. In this paper, the main models and the structure of the open-loop controller are described and validated. The controller is implemented in a rapid control prototyping device and validated reproducing real driving maneuvers at the engine test bench. Results of the online validation process are presented at the end of the paper.

**Keywords:** knock; combustion; efficiency improvement; $CO_2$ emissions; control; modeling



**Citation:** Brusa, A.; Cavina, N.; Rojo, N.; Mecagni, J.; Corti, E.; Ravaglioli, V.; Cucchi, M.; Silvestri, N. Development and Experimental Validation of an Adaptive, Piston-Damage-Based Combustion Control System for SI Engines: Part 1—Evaluating Open-Loop Chain Performance. *Energies* **2021**, *14*, 5367. https://doi.org/10.3390/en14175367

Academic Editor: Suhan Park

Received: 21 June 2021
Accepted: 23 August 2021
Published: 28 August 2021



## 1. Introduction

Knock presents a completely different challenge with respect to what is commonly faced when a standard dynamic system has to be controlled. The main reasons for this deep difference between knock events and other combustion phenomena can be synthetized as follows:

1. Lack of a robust relationship between values of knock intensity indexes and the associated damage on the combustion chamber components
2. Knock stochastic nature.

On one hand, numerous indexes for knock intensity estimation have been defined from the high-frequency content of measured or estimated in-cylinder pressure trace [1], from both high- and low-frequency ranges of such signal [2], or from high-frequency vibrations induced by abnormal combustions on the engine head. Regardless of the source of such signal and the mathematical formulation of the intensity index calculation, such indexes do not provide a direct indication about the consequences that every knocking event has on the combustion chamber, such as the erosion on the piston surface. On the other hand, the non-deterministic nature of knock forced the control system developers to define some statistical quantities, i.e., some percentiles values of certain knock index (typically higher than 90th) to manage the event rate over a given threshold [3], rather than the cyclic knock intensity, which closely approximates an independent random process. Consequently, real-time knock control has never been linked to actual component damage.

Knock intensity thresholds and criteria used for the spark advance (SA) calibration process are typically the result of the experience of the engine manufacturer and, in most cases, are defined to avoid knocking combustions at all. The highest percentiles (such as the 98th or the 99th) or even the cyclic intensity values are controlled to avoid the complete exceedance of some sort of experience-driven limit. Moreover, such thresholds may have remained the same over the years, not following the improvements in materials strength [4]. Indeed, improvements in alloys' mechanical characteristics have led to a significant increase of mean specific power, not necessarily followed by a corresponding redefinition of knock intensity thresholds. This is certainly caused by the lack of a robust quantitative relationship between calculated knock index, and corresponding induced damage.

Standard knock control strategies typically use signals coming from an on-board compatible system for knock intensity sensing (accelerometers or Ionization current-based, ION) and move spark advance at every time step. Spark timing is advanced whenever the intensity is lower than the threshold, while it is retarded when knock occurs, by applying fixed corrections [5–13]. Moreover, in some cases SA maps are calibrated to maintain knock intensity under the threshold for nominal operating conditions (environmental temperature, fuel Research Octane Number, RON, and so on), and by using the knock controller just to retard SA when the on-board system senses "high" intensity knocking events, according to defined spark timing correction maps [14]. SA retarding is then gradually reduced, reaching again the mapped value: this kind of controller is the so called "sawtooth".

More generally, traditional controllers' performance under transient conditions strongly depends on values of calibration constants [15–19]. Often, on production systems, standard controllers do not manage spark timing to reach a statistical knock index target value [20], such as a percentile of maximum amplitude of pressure oscillation (MAPO). It is more common having a controller that keeps such percentile under a calibrated threshold [21,22]. On the other hand, even under steady-state conditions, the actuated mean SA may be sub-optimal due to the high spark-timing variance. For these reasons, in most cases, such controllers are additionally calibrated with a precautionary approach, and this leads to a further combustion efficiency loss. In summary, two controlling issues can be traced in the following way:

1. The definition of a threshold for statistical knock indexes that are defined independently from the consequences induced by knocking events
2. The implementation of closed-loop controllers that have an output affected by a certain delay with respect to an open-loop-based strategy, especially when an engine runs under fast transient conditions.

The knock control algorithm proposed in this work can be considered as a solution to solve both issues, and the two key tools that allow managing combustion phasing in an innovative manner are the control-oriented piston damage model [23] and the analytical knock model [24]. Such controller is designed and developed for specific applications (racing, final vehicle development phase, test at the engine bench), or could represent the basis for introducing a closed-loop correction, in terms of adaptive capability to varying environmental conditions and aging effects (see Part II). Implemented models are developed and validated in previously cited works of the authors, but their features and latest updates are also reported in this work, which for the first time integrates the two portions and introduces a new, finite element method-based approach for the piston temperature model.

The piston damage model [23] was designed for the real-time (RT) estimation of the piston surface erosion, that is calculated as a function of its temperature and MAPO, while the knock intensity model [24] analytically defines the relationship between a calibratable MAPO percentile and the maximum in-cylinder pressure (Pmax), for any given operating condition (i.e., engine speed, load, target value of lambda and fuel quality). Both models can be considered as an innovative contribution to the field of knock modeling and control, especially because they allowed the development of the complex open-loop control chain described in this document that has the capability of converting a target piston damage

into a combustion phase value, cycle-by-cycle. The 50% of mass of fuel burned (MFB50) control-oriented model already described in a previous work of the authors [25] is here reversed to use target MFB50 as input and directly calculate the corresponding spark timing to reach such combustion phase value, for any given operating condition.

In this first paper (Part 1), a pure model-based, open-loop controller is developed and validated, and all combustion indexes needed to control combustion and piston damage (MFB50 and MAPO, respectively) are provided by analytical control-oriented models. The novelty introduced by the proposed solution with respect to the cited approaches is the integration of an innovative piston damage controller within a combustion one, which directly manages the instantaneous piston damage speed used as a knock intensity index alternative to MAPO. In this way, a much lower efficiency loss occurs under knock-limited operating conditions, due to a higher actuated SA with respect to standard calibrated values. Indeed, the latter is automatically defined as the value that generates an admissible piston damage speed. Results demonstrate the open-loop chain can reach target MFB50 with an extremely high accuracy even under transient operating conditions. The instantaneous knock intensity is evaluated through a novel index (piston damage speed), and it is directly controlled without applying any statistical methodology or buffer, as performed instead by standard knock controllers. It is important to anticipate that a predicted percentile of MAPO is used to feed the analytical knock model, but it is an index evaluated through a direct calculation, and it is updated once per cycle. It is not calculated with a buffer and thus, no delays are introduced in the control algorithm.

With the knock control strategy proposed in this work, the authors are thus proposing a solution for both issues listed above:

1. The target value of MAPO percentile derives from the admissible piston damage in a certain amount of time (i.e., a target piston damage speed), and this means it is defined according to the existing relationship between knock intensity and induced damage. Pmax and MFB50 models convert such value in a target combustion phase
2. With the open-loop chain the target MFB50 can be achieved by calculating the required SA. The controller is thought to be cycle-resolved, which makes such an algorithm suitable to accurately manage the combustion phase cycle-by-cycle even under transient conditions.

Outside knock limited operating range, the MFB50 model continues to calculate SA to maintain the combustion phase close to the target value. When the target MFB50 (the value that guarantees the target piston damage) is lower than such calibrated value, the MBT combustion phase becomes the actual target. For this reason, such a controller efficiently integrates both knock controller and combustion phase management.

A detailed description of model development and an assessment of model accuracy is reported in previous works of the authors [23–25].

However, it is important to mention the described pure open-loop controller cannot estimate accurate combustion indexes when events that are not considered by models occur. For instance, engine and exhaust system aging or extreme environmental conditions could have unpredictable effects on the combustion process, and thus on the calculated combustion phase and knock intensity. However, the presented models can be further developed to introduce dependency to such kinds of events, and this becomes particularly important when the engine is installed on a production vehicle. Indeed, the proposed open-loop combustion controller can be applied to conditions where extreme environmental conditions are avoided, and the engine has a limited life (such as at the test cell or during racing events), or it should be supported by a closed-loop controller for adapting to varying external conditions. Of course, the availability of a measurement of such indexes can prevent undesirable events and guarantees having a more robust algorithm (and this is the focus of Part II of this activity) for standard applications. Nevertheless, a pure open-loop control strategy developed in this paper represents an innovative solution and it is concretely used for special applications. Results are valuable and the presented tests demonstrate the general validity of the proposed approach. Moreover, authors can

anticipate that the closed-loop chain introduced with Part II of this activity is calibrated to react for protection reasons (i.e., just with negative SA corrections), and it is not active in most cases. In other words, even when the closed-loop is available, it reacts rarely and with small corrections (averagely −1 crank angle degrees of magnitude), and the controller still works mainly with open-loop chain.

The experimental setup and the database used for model calibration and validation are described, and each model is then briefly introduced below. The open-loop combustion controller is described in detail. The controller is then implemented in a rapid control prototyping (RCP) device and validated online at the engine test bench. Tests are carried out by reproducing engine speed and load profiles recorded during real vehicle maneuvers performed on track. Results are finally collected and discussed in the last part of the paper.

## 2. Experimental Setup

Experimental tests for model calibration and controller validation are carried out on a high-performance, 8-cylinder, Gasoline Direct Injection (GDI) and Turbo-Charged (TC) production engine. Each cylinder is equipped with a piezoelectric pressure transducer. The main engine characteristics and the layout of the development network used to test the complete controller via RCP are presented in Table 1 and Figure 1, respectively. The combustion chamber of this engine is characterized by a central spark plug and a side-mounted fuel injector. The indicating system is composed of CHAMPION charge amplifiers and OBI-M2 indicating system, both provided by Alma Automotive S.r.l. (Bologna, Italy), that are used for signal conditioning and acquisition, respectively. The indicating system acquires in-cylinder pressure signals at 200 kHz. Calculation of MFB50, indicated mean effective pressure (IMEP) and Pmax combustion indexes use the low-pass filtered pressure trace, while the same signal is windowed and band-pass filtered (specific cut-off frequencies and angular window cannot be disclosed for confidentiality reasons) to calculate MAPO, as defined by Equation (1):

$$\mathrm{MAPO} = \max(|p_{filt}|) \quad (1)$$

where $p_{filt}$ is the band-pass filtered, in-cylinder pressure signal. In the following text, the nomenclature "MAPO" or "knock intensity" indicates cyclic values of such an index, while, if it refers to a percentile value, it is always specified or it appears as "MAPO98" or "MAPO99.5" (for the 98th and the 99.5th percentile, respectively) or as "statistical knocking level".

**Table 1.** Eight-cylinder engine characteristics.

| Displaced Volume | 3.9 L (8 Cylinder) |
|---|---|
| Stroke | 82 mm |
| Bore | 86.5 mm |
| Connecting rod | 143 mm |
| Compression ratio | 9.45:1 |
| Number of valves per cylinder | 4 |

As mentioned above, the combustion controller has been tested through its deployment in an RT machine for RCP application that communicates with the ECU. The controller receives via the ECU the main engine parameters (such as speed, load, etc.), and it calculates for each cylinder a SA correction with respect to the mapped value. The models implemented in the open-loop controller calculate the combustion and knock indexes needed to determine spark advance corrections, and the indicating system is used to monitor the combustion process and to log in-cylinder pressure curves.

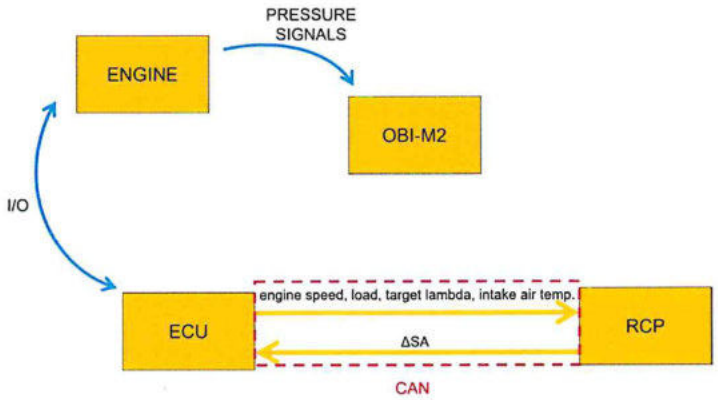


**Figure 1.** Functional layout of communication loop.

Data used for the controller validation were recorded during tests that reproduced different, real-use engine speed and load profiles from in-vehicle acquisitions. On the other hand, the database used for calibration of the analytical models (such as knock, Pmax, and MFB50 models) comes from an engine experimental campaign, needed to calibrate some ECU control strategies. In other words, such combustion data were not logged for this specific modeling activity but were already available. The piston damage model was calibrated instead with data recorded with the same 8-cylinder engine during a dedicated experimental campaign, described below. In the following sections, the main engine variables have been normalized with respect to their maximum value for confidentiality reasons.

## 3. Implemented Models

In this section, the piston damage model, the analytical knock intensity model, Pmax, and MFB50 models are described, highlighting those features that have to be considered to understand the development of the combustion controller. The results presented below are only a portion of the complete campaign carried out to develop each model, described in the previous works by the authors [23–25]. In this case, analytical models (knock, Pmax and MFB50) are specialized for each cylinder. This approach is needed to accurately control damage speed and combustion phase also including the cylindrical variability that is always present in multi-cylinder engines.

Knock, Pmax, and MFB50 models were developed to analytically describe the effects of engine operating conditions and other influent parameters, such as lambda and fuel RON (especially for the knock model), on a certain MAPO percentile, on maximum in-cylinder pressure, and combustion phase, respectively. They are developed by applying the separation-of-effects method [26] and only the engine parameters that significantly change when engine runs and that effectively affect such combustion indexes are included in these models. Valve timing, for instance, is an engine actuation that has a strong impact on the combustion process, but the variable valve timing (VVT) map is one of those calibrations that rarely changes, and it can be considered frozen after ECU calibration. Spark timing and lambda are varied by specific strategies that react to manage, for instance, catalyst heating, turbine inlet gas temperature, as well as traction of the vehicle and so on, and for this reason, the effect of lambda and SA changes must be counted by the models. On the contrary, fuel quality and intake air temperature are uncontrollable variables that undoubtedly change during vehicle life. These variables affect both knock tendency and SA-MFB50 relationship, and for this reason, RON of fuel available has to be correctly provided by the operator by calibrating the related variable, while air temperature is communicated to the control algorithm via CAN by ECU. Nevertheless, adaptive strategies are developed and presented in the second paper focused on this topic and they lead to automatically calculating current fuel RON so as to include its effects on the calculation of the final SA. The proposed approach is focalized to include only the parameters that can be significantly changed during the engine operation. Such a method for the prediction

of the effect of operating conditions variation on combustion indexes can be considered robust and reliable, especially when the final purpose of the modeling activity is that of developing control-oriented algorithms for a production engine.

Analytical models need to be calibrated when they have to be applied to a different engine, but as mentioned above, the data used to perform such a process come from a standard engine characterization database. Variables needed for model calibration are engine speed, load (evaluated as stoichiometric trapped air mass, (STAM)), SA, target lambda, fuel RON, MFB50, Pmax and MAPO and the process (that takes a couple of minutes) is based on the execution of a script that identifies the optimal coefficients of each model. Indeed, the formulation of each model is pre-defined, and only some specific coefficients need to be recalibrated for a different engine. On the other hand, piston temperature and damage models are developed following a physical approach. The piston temperature model can therefore be easily recalibrated by updating the piston geometry. As described below, the chosen piston finite element method (FEM) model approximates the piston shape as a flat plate, and thus only the thickness must be updated. Instead, the piston damage model is strongly related to the alloy with which the piston is made. For this reason, it can be applied to a different piston by comparing hardness curves of the two different alloys and properly scaling the corresponding coefficients.

Figure 2 shows the scheme of the complete algorithm, to anticipate the role of each model within the control strategy. The model-based controller converts the target damage speed into a target MFB50, and it is solved once per cycle, for each cylinder. The MFB50 and knock model provide combustion phase and knock intensity index to the piston temperature and damage models, respectively. The target damage speed is then converted into a target 98th percentile of MAPO, to properly feed the inverted knock model (the model inversion is highlighted with exponent -1 in the scheme). Finally, the inverted Pmax model outputs the target value of the combustion phase, and the reversed MFB50 model can directly calculate the SA correction needed to reach the target MFB50. The whole algorithm is solved through a direct calculation, and each index or target value is updated every cycle. The models implemented in such controllers are described in this section.

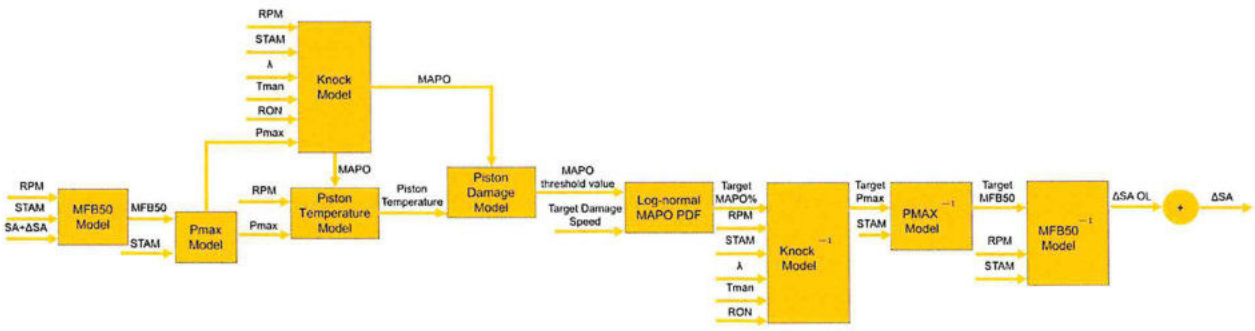


**Figure 2.** Complete open-loop controller scheme. All inputs needed by each model are reported.

### *3.1. Damage Model*

The piston damage [23] has to be evaluated by counting the effect of piston temperature, that changes the piston alloy resistance which is then damaged by knock-induced mechanical stress [27–30]. Figure 3 shows the decay of aluminum alloy hardness as a function of exposure time at different mean temperatures. Such a figure represents a material characteristic and Brinell hardness (HB) is reported on the *y*-axis.

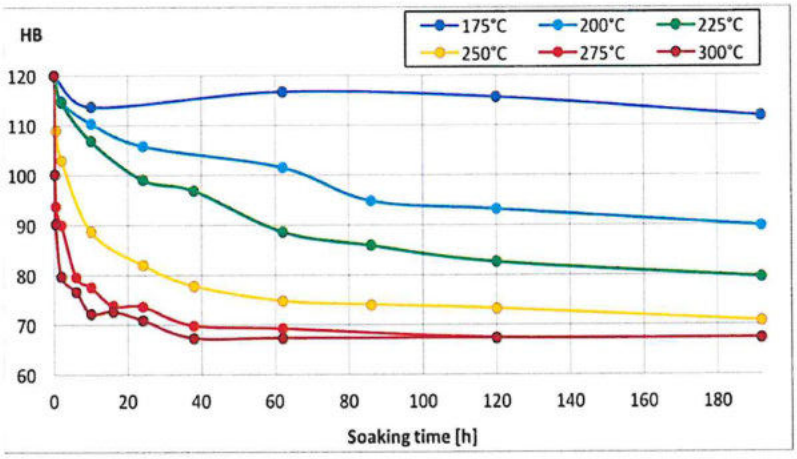


**Figure 3.** Hardness-temperature-time (HTT) curves for the aluminum alloy.

Development and calibration of a physical control-oriented piston temperature model for aluminum pistons (those mounted in the 8-cylinder engine considered in this work) precedes the discussion of the damage model. Tests for identification and calibration of both models are carried out on-engine in steady-state conditions, at 6000 RPM and 19.8 bar of brake mean effective pressure (BMEP), targeting a fixed knock level, (defined as a value of a MAPO percentile). Only 4 cylinders at a time are operated, and knock intensity is controlled independently for each cylinder. The tests were performed with RON 95 (cylinders 1–4) and RON 91 (cylinders 5–8) gasoline, and for different time intervals for the two engine banks (7.5 h for pistons 5–8 and 10 h for pistons 1–4). Target levels of statistical knock intensity were different for each cylinder, and for both engine banks. In addition, cylinder 5 was operated knock-free to have a reference condition. Such tests have been performed under steady-state conditions and the statistical knocking level was defined by using the 99.5th percentile of MAPO, that was evaluated on a buffer of 200 elements.

With the analysis of both in-cylinder pressure traces recorded during tests and piston damage, a predictive control-oriented piston damage model that is compatible with RT execution was then developed. Inputs are engine speed, Pmax, and MAPO, while output is the instantaneous damage speed, calculated as the cyclic damage induced by a single knocking event divided by the engine cycle duration. Of course, the same algorithm is applied for each cylinder. The layout of the resulting damage model is shown in Figure 4.

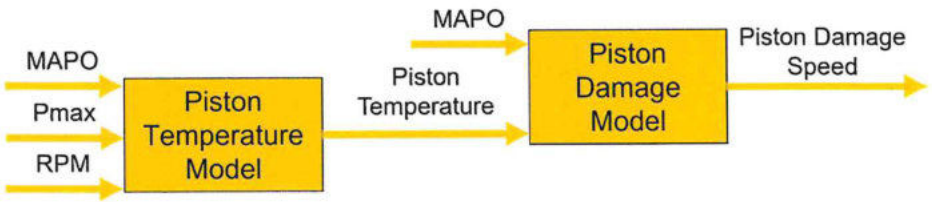


**Figure 4.** Scheme of piston damage model with logic blocks.

Residual hardness analysis on damaged pistons was carried out by performing micro-Vickers tests on the piston crown, considering 5 measurement locations on the intake side, and 5 on the exhaust side. Deep visual investigations were conducted with a digital microscope to determine the damage morphology in the area of the exhaust valve pockets and top-land, that are particularly sensitive to knocking erosion damage and which are where erosion was actually found. Roughness tests were also carried out in order to quantify the visible damage in the same areas.

By performing tests with different fuels (RON 91 and RON 95 gasoline) it is possible to separate the contributions of the heat transfer induced by the combustion process, and the additional amount due to knock. This evaluation is important to accurately determine

the piston surface temperature, hence the piston erosion. Indeed, if two cylinders are controlled to have different knocking levels with a fixed type of fuel, they necessarily experience different maximum in-cylinder pressures (due to a different spark timing) and wall thermal load, regardless of knock intensity. Consequently, differences in measured thermal effects on pistons (residual hardness) are not fully attributable to knock, because they depend on both different Pmax and knock intensity (always evaluated as the 99.5th percentile of MAPO). Thus, combustion-related and knock-related heat transfer rates cannot be separated by moving spark timing only. The use of fuels with different RON numbers enables obtaining the same Pmax level by applying the same SA with different knock intensities, and vice versa. Thus, the proposed method is needed also to quantify and calibrate the temperature role in the damage mechanism by controlling, for example, different piston temperatures at the same knock intensity. Further details about such considerations are provided by the authors in [23].

The mean piston surface temperature can be estimated by measuring residual hardness after the tests on 5 spots on each side, and by using the hardness-temperature-time curves (Figure 3). These measurements show non-uniformity in the temperature field, both on the intake and exhaust side. Nevertheless, the measurements turned out to be symmetrical with respect to the thrust-antithrust axis of the piston surface geometry. Symmetry can therefore be used to average the measurements. In this way, as shown in Figure 5, for every piston it is possible to calculate 6 global hardness values, of which 4 are averaged, while the remaining 2 are calculated according to the thrust-antithrust axis. This approach significantly simplifies the piston temperature model, without excluding the spatial temperature range on the piston crown. Such observations are used for piston temperature model calibration.

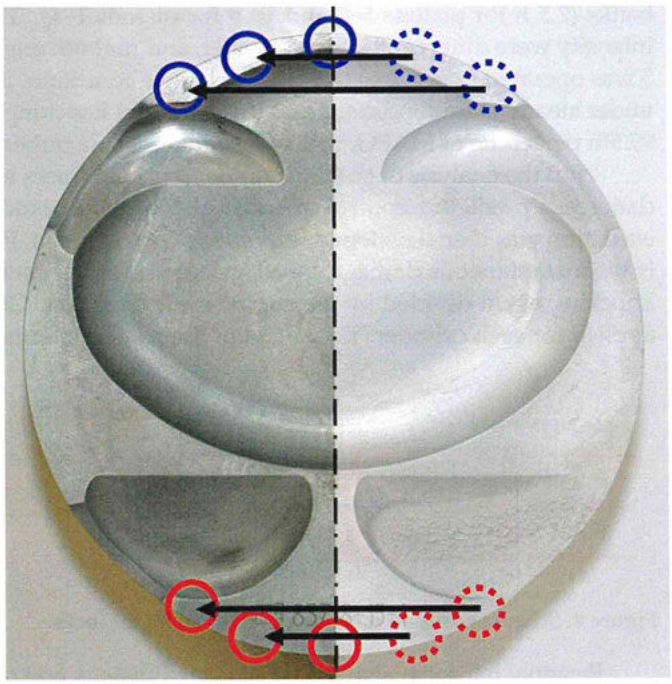

**Figure 5.** Hardness measurements symmetry, used to average homologous locations.

The temperature model was then developed according to the following hypotheses:

1. Even if the heat transfer rate on both piston surfaces (the combustion chamber and the sump ones) changes by orders of magnitude during the combustion cycle, the skin piston temperature can be supposed to be almost constant during the cycle, due to the high conductivity and the specific heat of the material. The model is therefore computed once per cycle.

2. The exchange condition between gas and piston crown is assumed to be uniform on the entire surface. The specific heat flux is imposed on the piston surface, which assumes that heat transfer is not dependent on surface temperature. Albeit inaccurate, this is deemed to be an acceptable simplification for calculation purposes because the piston temperature is lower than the gas space-averaged temperature.
3. Oil jets cooling is assumed to be the only active path of piston heat rejection (it represents 60% of the total heat rejection, according to [31–33]), so that the heat exchange through the ring belt and the skirt is neglected. These contributions are acknowledged not to be negligible, but their calibration would require, for example, to conduct tests with different coolant temperatures (and to perform the resulting hardness measurements). Conductive heat transfer is very complex and difficult to investigate with specific experimental tests, and for this reason, it is simplified by supposing that the piston bottom inner surface is involved in the heat exchange process and most of such process takes place in the surface directly touched by the oil jets. Figure 6 shows the method for the estimation of the distance between different locations on the piston surface and the area touched by the oil jets.
4. The ratio between gas-exposed (upper) and oil-impinged (lower) areas is unitary, which means that in stationary conditions the specific heat flux across the thickness is uniform, and the heat flux is mono-dimensional. Substantially, it is equivalent to a flat plate, but with differential thermal conductivity (because of the varying distance between the two sides in the real piston).

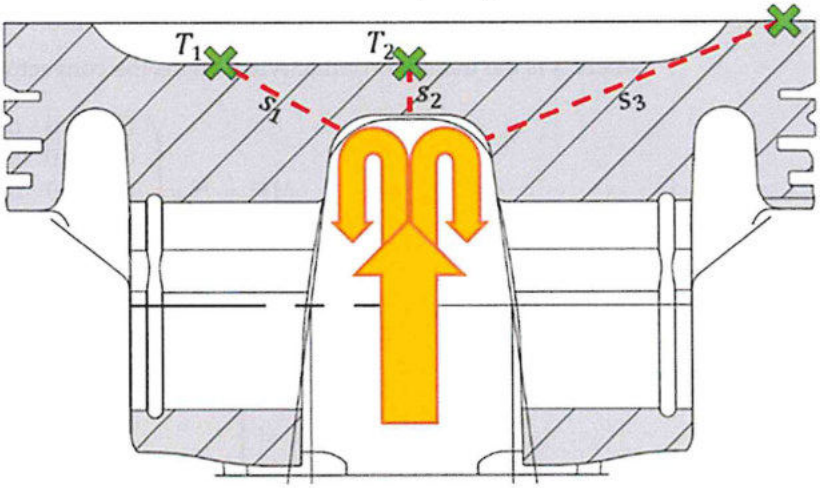


**Figure 6.** Qualitative oil jets position, used for the estimation of the measurement location distance from the oil-impinged surface.

The result is a non-stationary finite-element model [34,35], where nodes are distributed along the thickness of the piston, and an equivalent thickness is defining the location. Such parameter is the only one that needs to be updated for the piston temperature model recalibration when a different engine geometry is considered. The boundary conditions are the same for every measurement location (i.e., resulting thickness) considered:

- imposed heat flux on the gas side (Neumann condition)
- conductive heat transfer on the oil side (Robbins condition)

The temperatures in the nodes $T_t$ at time $t$ are calculated by:

$$T_t = MM \backslash FF \tag{2}$$

With $MM$ and $FF$ defined by Equations (3) and (4):

$$MM = \frac{MC}{ts} + \alpha\,(MK + MH) \tag{3}$$

$$FF = \left(\frac{MC}{ts} - (1-\alpha)(MK + MH)\right) T_{t-1} + F \tag{4}$$

where:

- $\alpha$ defines the method: 0, 1, 0.5 for explicit, implicit and Crank-Nicholson, respectively
- $ts$ is the time-step
- $T_{t-1}$ is the temperature vector at the previous time-step $t-1$
- $MC$ is the capacity matrix

$$MC = \frac{\rho\, c\, l}{2} \begin{pmatrix} 1 & 0 & 0 & 0 & 0 \\ 0 & 2 & 0 & 0 & 0 \\ 0 & 0 & 2 & 0 & 0 \\ 0 & 0 & 0 & 2 & 0 \\ 0 & 0 & 0 & 0 & 1 \end{pmatrix} \tag{5}$$

where $\rho$, $c$ and $l$ are the density, the specific heat, and the elements length, respectively. $MK$ is the conductivity matrix:

$$MK = \frac{\lambda}{l} \begin{pmatrix} 1 & -1 & 0 & 0 & 0 \\ -1 & 2 & -1 & 0 & 0 \\ 0 & -1 & 2 & -1 & 0 \\ 0 & 0 & -1 & 2 & -1 \\ 0 & 0 & 0 & -1 & 1 \end{pmatrix} \tag{6}$$

where $\lambda$ is the material conductivity. $MH$ is the convective matrix:

$$MH = H_{oil} \begin{pmatrix} 0 & 0 & 0 & 0 & 0 \\ 0 & 0 & 0 & 0 & 0 \\ 0 & 0 & 0 & 0 & 0 \\ 0 & 0 & 0 & 0 & 0 \\ 0 & 0 & 0 & 0 & 1 \end{pmatrix} \tag{7}$$

where $H_{oil}$ is the convective coefficient at the oil-piston boundary. $F$ is the vector of the loads:

$$F = \begin{pmatrix} q_{pist_t}\, \alpha + q_{pist_{t-1}} (1-\alpha) \\ 0 \\ 0 \\ 0 \\ H_{oil} T_{oil} \end{pmatrix} \tag{8}$$

In which:

- $q_{pist_t}$ is the specific heat flux at the gas-piston boundary at time $t$;
- $q_{pist_{t-1}}$ is the specific heat flux at the gas-piston boundary at time $t-1$;
- $T_{oil}$ is the oil temperature.

$H_{oil}$ is an unknown model parameter, such as $q_{pist}$. The heat transfer problem is represented in Figure 7, and it needs to impose $H_{oil}$ or $q_{pist}$ to be solved. In the figure, piston and oil-piston interface are two thermal resistances connected in series.

Under steady-state conditions, $H_{oil}$ can be calculated through Equation (9) from piston temperature, piston thickness $s$ (evaluated by analyzing the piston geometry) and specific power $q_{pist}$ [36]:

$$H_{oil} = \frac{1}{\frac{T_{crown} - T_{oil}}{q_{pist}} - \frac{s}{\lambda}} \tag{9}$$

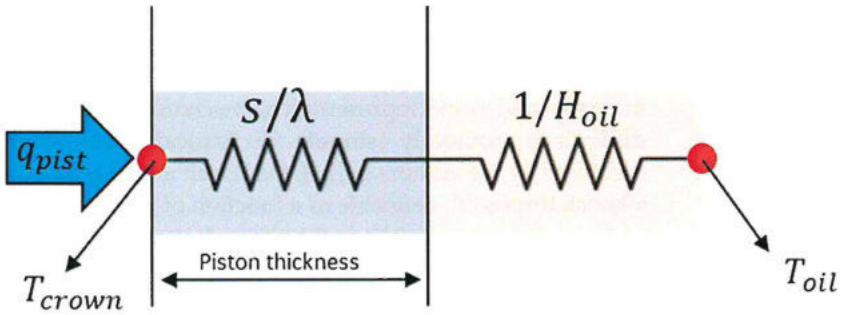


**Figure 7.** Schematic representation of heat transfer through thermal resistances series.

The mean value of the specific heat flux within the combustion cycle, $q_{pist}$, is imposed on the gas side and it is estimated by a linear empirical correlation, with the maximum pressure of the cycle and the engine speed as inputs. This is supposed to be valid in non-knocking combustions, while an additional contribution is given by knock, but through a localized effect. For this engine, piston damage was observed on the exhaust side, so it is assumed this is the location where knock occurs. Consequently, the knock-related heat transfer contribution is to be considered only on the exhaust side. Thus, the specific power model, $q_{pist} = f$(Pmax, RPM, MAPO), is defined as a linear function of Pmax and engine speed. Moreover, for the exhaust side, it is multiplied by a term linearly increasing with MAPO:

$$q_{pist} = (a\ \mathrm{Pmax} + b\ \mathrm{RPM} + c)K_{\mathrm{MAPO}} \tag{10}$$

where $K_{\mathrm{MAPO}} = 1$ for the intake side and $K_{MAPO} = \max(\mathrm{MAPO} - 4,\ 0)d$ for the exhaust side, and $a$, $b$, $c$, and $d$ have to be identified.

$K_{\mathrm{MAPO}}$ definition is thought of as a line with positive slope, passing through MAPO = 4 and saturating at 0. The meaning is that cycles with a MAPO value lower than 4 (an arbitrary and calibratable threshold) are not increasing the nominal $q_{pist}$ value, while higher values of MAPO are amplifying such an amount.

In Figure 8, the calibration process is summarized. Combustion indexes (Pmax and MAPO) recorded during bench tests are vectors describing the whole pressure history (one value for every combustion cycle) experienced by the piston. The piston temperature model estimates the temperature history (one value for every cycle) for every measurement point. Then, with the HTT curves seen in Figure 3 the hardness history for every measurement point can be estimated by using data about cumulative exposure time and mean temperature. Finally, the residual hardness values are compared to the measured ones. This is applied to every tested piston. To minimize the cost function, which is defined as the sum of all the absolute errors, for every piston, for every measurement point, *fminsearch* function in MATLAB (R2018, MathWorks Inc., Natick, MA, USA) optimization toolbox [37] is used.

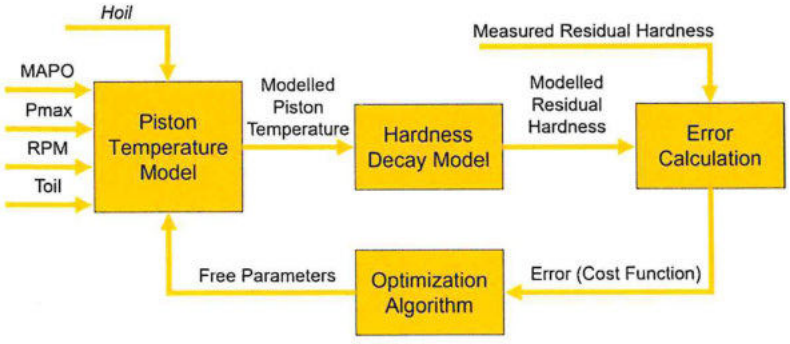


**Figure 8.** Calibration process for the piston temperature model.

Knock damage model inputs are thus MAPO, representing the mechanical stress acting on piston surface, and piston surface temperature, from which piston alloy resistance strongly depends (Figure 3). Some sort of linear dependence between measured knock intensity and some representative mechanical stress values is assumed since it is very difficult to accurately estimate mechanical forces on piston surface due to knock. As described by the authors in [23], the knock model is based on the consideration that there is a knock threshold, definable as a function of piston surface temperature, beyond which the material deformation falls in the alloy plastic field. Such threshold is therefore calibrated in this model.

Temperature dependence is obtained by moving plastic field boundary (i.e., knock index threshold), while the plastic slope is assumed to be constant. The total modeled damage is given by the summation of the corresponding damage of every cycle. The model calibration consists of the identification of 2 parameters (the gain and the offset of linear MAPO threshold with respect to piston temperature). The calibration algorithm is schematized in Figure 9, and it is very similar to the one adopted for the piston temperature model. Model inputs are MAPO and the piston temperature, updated with engine cycles frequency. The cost function (CF) is defined to maximize Pearson's correlation, ρ, between the measured and the modeled damage D:

$$CF = 1 - \rho(D_{meas}, D_{mod}) \tag{11}$$

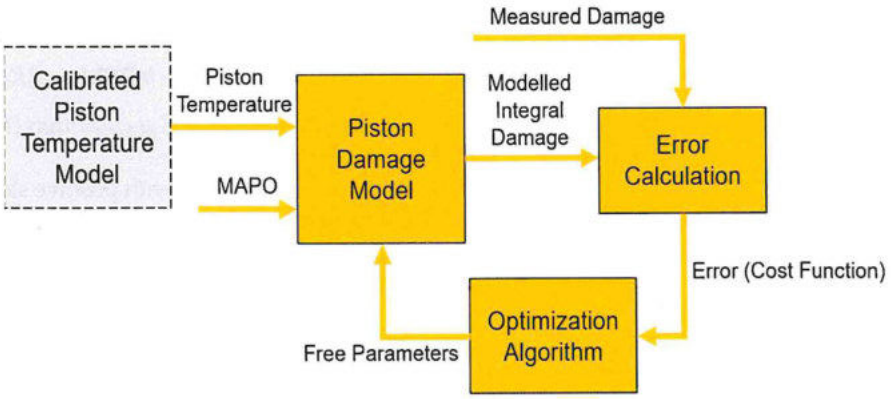


**Figure 9.** Damage model calibration process.

The best configuration found for the knock index threshold dependence on temperature is reported in Figure 10, which is also the adopted threshold map.

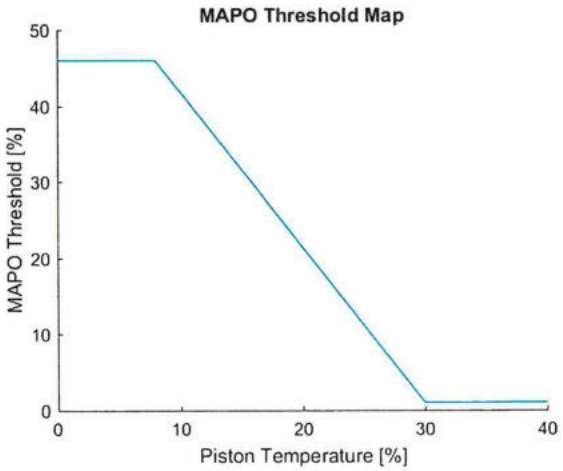


**Figure 10.** MAPO threshold as a function of normalized piston temperature.

Model calibrations clearly depend on piston alloy characteristics. This means that the whole approach can be easily calibrated for a different engine with the same piston alloy, by just updating piston thickness, for the area in which knock-induced erosion occurs. Once such an area is identified and the piston geometry is known, the methodology can be adapted for another engine. By comparing the online MAPO values and the calibrated threshold for given piston temperature, the excess over the threshold can be calculated for every cycle, estimating the induced damage in the piston exhaust valve pockets and top-land. The calculated damage represents the amount of pressure (MAPO) that exceeds the threshold, and it can then be expressed in *bar*.

At this point, the corresponding allowable knock intensity, and the resulting engine performance, have to be spread throughout engine life. Indeed, an accelerated damage generation and the corresponding performance increment over a short time would be a very inefficient way of using this model, and it could also result in non-uniform engine performance achievable by the driver over time. Moreover, if the target of the model would be defined as the cumulative piston damage evaluated at the end of engine life, the controller would reach too severe knocking combustions, especially after a period in which the calculated damage is zero (for instance, due to a drive with a low torque request). Of course, this is an undesirable behavior due to the high knocking levels that could cause the engine seizure. For such reason, rather than the cumulative damage at the end of engine life, the control strategy target should be a constant damage speed, which finally generates the desired damage level upon completion of the design life cycle. The acceptable piston erosion has been experimentally established by the engine manufacturer, by verifying the maximum damage that does not compromise any engine functional parameter. On the other hand, even the time of the engine life spent under knock-limited operating conditions (i.e., engine points for which it could be reached the target damage speed) has been determined by the engine manufacturer, through a market investigation that figured out the behavior of the "mean" driver of the vehicles that mount the considered engine. Thus, supposing a predefined time of the engine life spent under knock-limited operating conditions, $Life_{tgt}$ (expressed in seconds) and a target modeled damage (that derives from the maximum admissible piston damage evaluated at the end of engine life), $Damage_{tgt}$ (expressed in *bar*), a damage speed target $DS_{tgt}$ can be defined, as described in Equation (12):

$$DS_{tgt} = \frac{Damage_{tgt}}{Life_{tgt}} \quad \left[\frac{bar}{s}\right] \tag{12}$$

Similarly, the estimated instantaneous damage speed can be defined as:

$$DS_{est} = \frac{Damage_{est_{|P}}}{P} \quad \left[\frac{bar}{s}\right] \tag{13}$$

where $P$ is the considered period and $Damage_{est_{|P}}$ is the damage per cycle estimated by the model. For the model implementation in the open-loop-based combustion controller, the period $P$ is the engine cycle time, that for a 4-stroke engine can be calculated with Equation (14):

$$P = \frac{2 * 60}{RPM} \quad \left[\frac{s}{cycle}\right] \tag{14}$$

The piston temperature model coupled with the damage model calculates the instantaneous damage speed, using engine speed, Pmax and MAPO as inputs. These models are the solution proposed by the authors for the first issue discussed in the Introduction. Indeed, they represent a validated and reliable control-oriented tool for the conversion of the cyclic MAPO value into the corresponding piston surface erosion. Thus, such an approach replaces the traditional knock intensity index used in calibration with a more significant and tangible damage index. However, MAPO remains a knock intensity index that can be directly measured through the in-cylinder pressure sensing system, while the piston surface erosion can be only calculated online through the model. In this work, the

cyclic MAPO value is calculated by the knock model, as described by the authors in [24]. For given operating conditions, the complete probability density function (PDF, see the Appendix of [24]) is determined and the cyclic MAPO value is extracted. Indeed, MAPO is needed by the piston damage model to calculate the piston temperature. Considering the final purpose of the feed-forward combustion controller (i.e., converting the target damage speed into a target combustion phase), the translation of the target piston surface erosion into a combustion index correlated with MFB50 is needed. The analytical knock model previously developed by the authors [24,25] becomes, thus, a useful tool to perform such a conversion, and for this reason, it is briefly described below. Its simple analytical formulation makes it particularly suitable to be implemented in a combustion controller for a production ECU. A MAPO percentile becomes the input and Pmax becomes the output, simply by reversing the standard model equation. Such percentile (that can be arbitrarily chosen) needs to be fed to the reversed analytical knock model, and it depends on MAPO threshold and, thus, on piston temperature.

Depending on both operating conditions and oil temperature, the FEM model described above estimates the piston temperature and based on this, the MAPO threshold between safe and damaging intensities is defined. Hence, for given MAPO threshold and for given target damage per cycle, the MAPO log-normal PDF that produces such damage can be univocally defined. The cyclic damage is calculated multiplying the damage speed with the time (expressed in seconds) of an engine cycle. It is then possible to calculate the cyclic knock damage as the integral of MAPO values over such threshold. Consequently, given the instantaneous estimated piston temperature and the target damage speed, the corresponding MAPO PDF (within the ∞^1 possible distributions, depending on operating condition) can be identified and converted into the value of a given MAPO%. For a certain MAPO PDF, the related damage per cycle is graphically represented in Figure 11 and it can be calculated through Equation (15):

$$Damage\ per\ cycle\ [bar] = \int_{THR}^{+\infty} (\mathrm{PDF}\ \Delta\mathrm{MAPO})\ \mathrm{dMAPO} = \int_{THR}^{+\infty} \mathrm{PF}\ \mathrm{dMAPO} \quad (15)$$

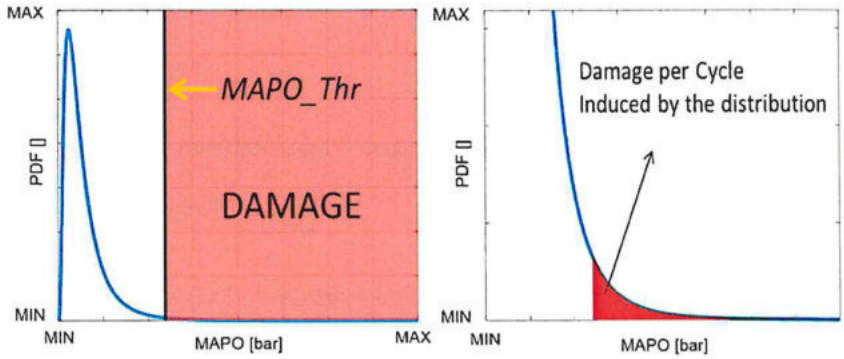


**Figure 11.** Damage per cycle associated to the MAPO distribution for the given MAPO threshold.

In which ΔMAPO is the interval used to discretize the MAPO domain and PF is the probability function.

An iterative calculation of the targeted PDF (and corresponding MAPO percentile) is implemented in the control strategy. As mentioned above, once the log-normal PDF that fits the integral value over the MAPO threshold calculated by the knock model is identified through Equation (15), the corresponding value of a MAPO percentile (98th in this case) can be used by the knock model as input. Such algorithm uses the linear function between two percentiles of a log-normal distribution introduced in the Appendix in [11] and reported in Equation (16):

$$\mathrm{MAPO50} = g\ \mathrm{MAPO98} \quad (16)$$

Based on the authors' experience, $g$ is fixed on the entire engine operating field, and it can be univocally determined by analyzing the ratio between MAPO50 and MAPO98. In other words, it is identified when the analytical knock model is calibrated for the considered engine and then it is kept fixed. In this way, it is possible to halve the independent variables that the iterative calculation has to change because once the value of MAPO98 is defined, MAPO50 can be calculated via Equation (16). Of course, the approximation of the MAPO for fixed operating conditions with a log-normal PDF introduces an error, but, as described in [24,38], such kind of function is one of the most accurate ways to describe the distribution of MAPO probability. The error introduced by such approximation is evaluated in detail in [24]. In this work, the focus is the development of the combustion controller and in the last part of this paper, the overall error (that incudes even the error introduced by each model) between targeted and measure values is reported. At the same time, when two percentiles are known (and one of these is 50th), the mean value ($\mu$) and the standard deviation ($\sigma$) can be directly calculated by using the properties of the log-normal PDF:

$$\mu = \ln(\text{MAPO50}) \tag{17}$$

$$\sigma = \frac{\ln(\text{MAPO98}) - \ln(\text{MAPO50})}{2.0057} \tag{18}$$

In other words, the procedure varies the highest percentile in a certain calibrated range (in that case 98th, but it can be arbitrarily chosen as a percentile higher than the 50th) and 50th percentile (directly deductible with Equation (17)) to find the MAPO PDF for which the integral value of knock index values over the threshold (defined by damage model) coincides with the cyclic target damage. This can be calculated by reversing Equation (13):

$$Damage_{tgt} = DS_{tgt}\, Life_{tgt}\ [bar] \tag{19}$$

Figure 12 shows the algorithm scheme, while Equation (20) indicates the mathematical expression of such an algorithm.

$$\text{MAPO98}_i = \text{MAPO98}_{i-1} + \left( Damage_{tgt} - \int_{THR}^{+\infty} (\text{PDF}_{i-1}\, \Delta\text{MAPO})\ \text{dMAPO} \right) \tag{20}$$

where $i$ and $i-1$ indicate the current and the previous iteration of such iterative calculation. However, an iterative procedure is not compatible with RT execution of the complete controller because it needs multiple iterations that must be completed between two consecutive engine cycles. Thus, this procedure was executed offline for a reasonable range of target damage rates and for several MAPO threshold values (Figure 10, and a 2-D lookup table was then calibrated. A direct calculation of target MAPO98 for a given MAPO threshold would be possible, but it would contain mathematical operations between values with different orders of magnitude and this would be numerically unsuitable for the final implementation in a production hardware. Thus, considering the limitations imposed by the final implementation on the ECU, such a kind of operations should be converted into a Lookup Table (LUT) that contains the result. For such reasons, the authors preferred to simplify the whole calculation of the target MAPO98 by introducing a map. The target damage speed and MAPO threshold are the inputs, while the target MAPO98 value is the output. At this point, it is clear how such MAPO98 is not calculated using a buffer (that would inevitably introduce a delay in the calculation), but it is applied just as an index for the conversion of the current MAPO threshold into a proper input for the reversed analytical knock model (that is briefly introduced in the following section). The whole control algorithm is thus characterized by direct calculations and there is not any kind of filter (buffers, moving averages, and so on). Even such a feature can be considered as a significant novelty in the field of knock control.

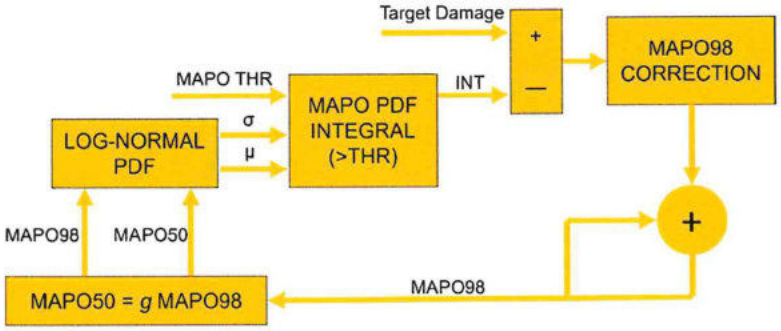


**Figure 12.** Block scheme of the algorithm used to find the MAPO PDF that achieves the target cyclic piston damage.

### 3.2. *Analytical Knock Model*

The analytical knock model is used to convert the target MAPO98 value into corresponding Pmax [24]. The choice of 98th percentile is arbitrary. It was chosen for the knock model calibration and, consequently, as the output of the iterative procedure described above because it represents a good compromise between numerical stability and sound representation of high-end MAPO values. Equation (21) shows the model analytical formulation for a standard GDI, TC engine:

$$\begin{aligned} \text{MAPO98\%} = {} & (a\ \text{STAM}^{b})\ (\text{Pmax} + ((\lambda - \lambda_{\text{ref}})\lambda\text{m}) + ((\text{T}_{\text{man}} - \text{T}_{\text{man\_ref}})\text{Tm}) \\ & + (\ (\text{RON}_{ref} - \text{RON}_{fuel}\ )\text{RON}m\ )\ )^{(c\ \text{STAM}+d)} + \text{RPM ESm} \end{aligned} \tag{21}$$

where:

- MAPO% is the MAPO percentile to be calculated
- $a$, $b$, $c$, and $d$ are the four calibration parameters of the model that allow the definition of MAPO% for the reference conditions (reference lambda value and air temperature in the intake manifold)
- STAM is the stoichiometric trapped air mass, which is equal to the trapped air mass (TAM) per cycle per cylinder when the mixture is stoichiometric or rich, and the ratio between TAM and lambda when the mixture is lean
- $\lambda$ is the current lambda value
- $\lambda_{\text{ref}}$ represents the reference lambda value, with which model coefficients ($a$, $b$, $c$, and $d$) are calibrated. In this case, $\lambda_{\text{ref}}$ is equal to 1
- $\lambda$m is the lambda multiplier, a calibratable coefficient that converts the lambda numerical difference in $\Delta$Pmax
- $\text{T}_{\text{man}}$ is the current air temperature in the intake manifold
- $\text{T}_{\text{man\_ref}}$ is the reference temperature in the intake manifold. In this case it is equal to 40 °C
- Tm is the intake air temperature multiplier, a calibratable coefficient that converts the temperature numerical difference in $\Delta$Pmax
- $\text{RON}_{ref}$ is the reference fuel RON value, used during tests which generated the database with which parameters $a$, $b$, $c$ and $d$ were calibrated
- $\text{RON}_{fuel}$ is the RON number of the current fuel
- RON$m$ is the fuel RON multiplier, a calibratable coefficient that converts RON numerical difference into $\Delta$Pmax, as well as the $\lambda$m.
- ESm is the engine speed multiplier, and it includes the effect of combustion noise as a function of engine speed.

As observable in Equation (21), the effects of the mixture enrichment and intake air temperature on MAPO are modeled as an additive contribution to Pmax value. The result can be seen as a mere translation of MAPO98% curve along the Pmax axis. In other words, for fixed engine speed, load, and fuel, when the mixture is enriched, or the intake air temperature is lower than reference, the same Pmax is achieved with a lower MAPO98

value. Such phenomenon is visible in Figure 13, in which normalized MAPO98% curves on Pmax axis are reported for three spark sweeps performed with the same engine speed, load (7000 RPM, 1800 mbar of intake manifold pressure) and type of fuel, but for different lambda values. Knock index is offset by the modeled engine speed contribution. Legend includes the lambda value, the intake air temperature, and the fuel RON, respectively. Of course, the same behavior can be observed when the intake manifold pressure varies.

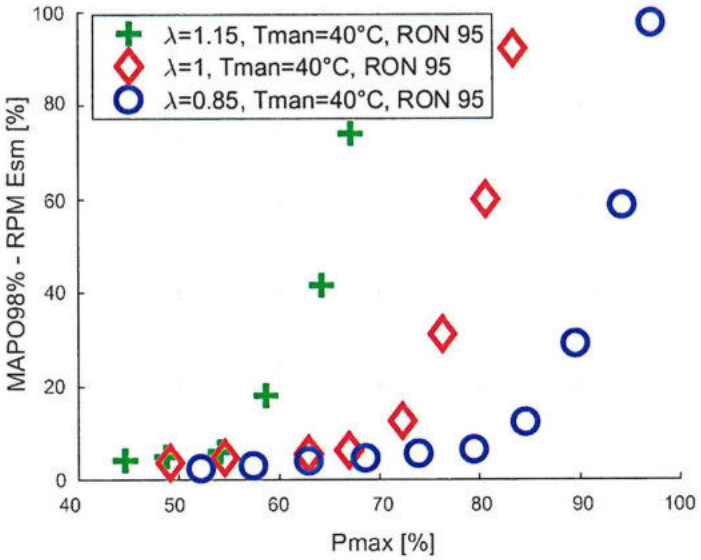


**Figure 13.** Normalized and offset MAPO98% curves for fixed operating conditions (7000 RPM, 1800 mbar of intake manifold pressure) but for different lambda values.

The same approach used to model the influence of lambda and intake air temperature on statistical MAPO98 is applied to include fuel RON variations. Indeed, as shown in Figure 14, a fuel RON increase acts as a mere translation of MAPO98 curves along Pmax axis, showing the same qualitative trend observed for mixture enrichment.

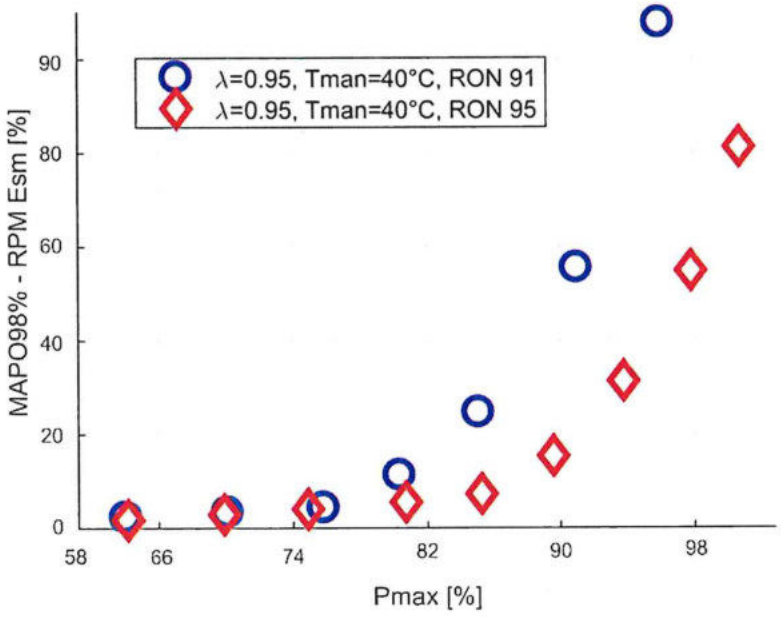


**Figure 14.** Normalized and offset MAPO98% curves for fixed operating conditions (7000 RPM, 1800 mbar of intake manifold pressure) for two fuel RON values.

Model equation is then reversed to convert a target MAPO98% into a Pmax value. Analytical formulation of such model is shown by the following Equation (22):

$$\mathrm{Pmax}_{tgt} = \sqrt[(c\ \mathrm{STAM}+d)]{\frac{(\mathrm{MAPO98\%_{tgt}}-\mathrm{RPM\ ESm})}{(a\ \mathrm{STAM}^{b})}} + (\lambda_{\mathrm{ref}}-\lambda)\lambda\mathrm{m} + (\mathrm{T_{man\_ref}}-\mathrm{T_{man}})\mathrm{Tm} + \mathrm{RONm}\left(\mathrm{RON_{fuel}}-\mathrm{RON}_{ref}\right) \quad (22)$$

where $\mathrm{MAPO98\%}_{tgt}$ is the target MAPO98 value determined by converting target piston damage and MAPO threshold into a MAPO PDF, and $\mathrm{Pmax}_{tgt}$ is the corresponding Pmax value, for fixed operating conditions. The model inversion can be performed without carrying out a new calibration process of model parameters ($a$, $b$, $c$, $d$, ESm and so on) and this is a further demonstration of the possibilities that derive from the analytical approach proposed by the authors.

### 3.3. Analytical Pmax Model

The control-oriented Pmax model was described and validated in a previous work of the authors [25]. The reversed analytical formulation of such a model can be easily implemented in the combustion controller to convert Pmax value into the corresponding MFB50. Equation (23) represents the standard model formulation. It is a first-order polynomial with respect to engine load (evaluated as STAM) and a second-order polynomial with respect to MFB50. This means that two possible solutions exist by reversing such an equation to calculate MFB50. Nevertheless, only the positive one defines the physical value of combustion phase. Thus, Equation (24) shows the proper formulation of the reversed Pmax model.

$$\mathrm{Pmax} = p_{00P} + p_{10P}\mathrm{MFB50} + p_{01P}\mathrm{STAM} + p_{20P}\mathrm{MFB50}^2 + p_{11P}\mathrm{MFB50\ STAM} \quad (23)$$

$$\mathrm{MFB50} = \frac{-(p_{11P}\mathrm{STAM}+p_{10P}) + \sqrt{(p_{11P}\mathrm{STAM}+p_{10P})^2 - 4\,p_{20P}(\mathrm{Pmax}+p_{00P}+p_{01P}\mathrm{STAM})}}{2\,p_{20P}} \quad (24)$$

The implementation of the reversed Pmax model in the open-loop combustion controller allows the determination of the target combustion phase that achieves the target damage speed. Figure 15 shows the controller layout at this point of the system development.

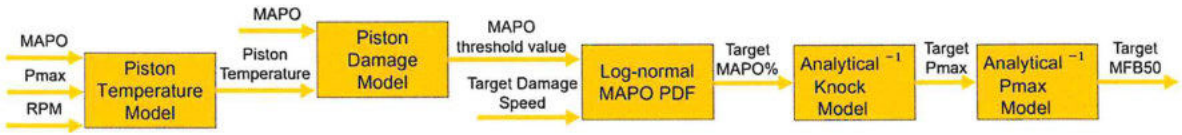


**Figure 15.** Controller layout including reversed Pmax model.

### 3.4. Analytical MFB50 Model

The final output of the open-loop chain is the ΔSA (with respect to mapped value) that achieves target MFB50. MFB50 model analytically defines the relationship between actuated spark timing and combustion phase [25]. Figure 16 represents the block scheme of the controller open-loop chain, including the reversed MFB50 model.


**Figure 16.** Controller layout including MFB50 model.

Such model is reversed with respect to what is described by the authors in [25] to calculate ΔSA. For each engine point (any given engine speed and load), the relationship between mean MFB50 and actuated SA has a parabolic trend, which can be described with

a second- order polynomial. Such trend derives from a variable MFB50 sensitivity to the SA: the higher the MFB50, the lower the curve slope. Figure 17 shows an example of what has been asserted, collecting data for a spark sweep recorded for fixed engine speed and load. SA is reported as the difference from the mapped value (ΔSA) and the MFB50 is normalized with respect to maximum value.

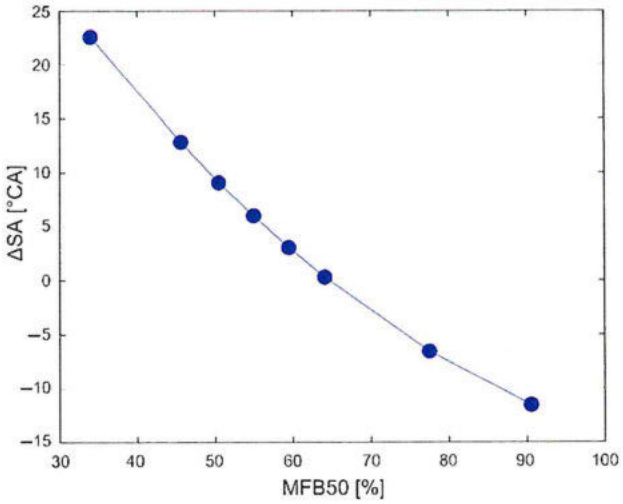


**Figure 17.** Experimental MFB50-ΔSA points recorded during a spark-sweep for fixed engine speed and load. MFB50 is normalized with respect to the maximum value.

Thus, for each engine point (speed and load), a second order polynomial can be calculated and the SA that univocally determines the target MFB50 value can be directly evaluated.

## 4. Open-Loop Combustion Controller Validation

The controller scheme shown in Figure 16 also needs cyclic Pmax and MAPO values as inputs of the piston temperature and damage model. Thus, the control system is further developed, by introducing a standard Pmax model defined by Equations (16)–(18), Equations (21) and (22), to calculate cyclic MAPO value. Such model implements the algorithm that defines the MAPO PDF as a function of engine speed, load, Pmax (and thus spark timing), lambda, intake air temperature and fuel RON. Once the PDF is known, the model extracts some values randomly but according to the probability determined by such PDF. Such operation is carried out by using the Matlab/Simulink random function and specifying the mean value and the standard deviation of the current log-normal distribution [37]. In this way, even the random behavior of MAPO is reproduced. The output of knock model block is thus the instantaneous MAPO, needed by the piston damage model to evaluate the corresponding piston temperature (and thus the target MAPO threshold and the corresponding MAPO98), calculated once per cycle. Moreover, Pmax model needs current MFB50 as input and for such reason also the MFB50 analytical model is added to the final controller scheme. Of course, in this case, the polynomial equation described by the authors in [25] is implemented to calculate the MFB50 when SA is given. The scheme shown in Figure 16 evolves into that anticipated by Figure 2. The spark advance that is used as input for the standard MFB50 model (left-hand side of Figure 2) is the value that results by adding the mapped value with the correction calculated by the controller for the previous combustion (right-hand side of Figure 2).

The resulting combustion controller is finally implemented in an RCP system. The complete open-loop controller is available for each cylinder, and it uses current engine operating parameters (engine speed, STAM, target lambda and mapped SA) communicated by ECU via CAN, and modeled combustion indexes.

The engine at the test bench is operated with speed and load profiles recorded during real vehicle maneuvers. The tested profiles consist of complete track laps and include both

very steep transients and semi steady-state conditions. In this way, controller is stressed with realistic engine speed and load profiles, and results demonstrate the high reliability of the proposed tool on the entire engine operating range and for all the operating conditions. Tests were performed with RON 95 fuel, and such value is manually tuned and kept fixed.

Figure 18 shows the engine speed and pedal traces of an exemplary profile tested during the validation procedure, normalized with respect to maximum values of the engine operating range. Thus, the entire engine operating field is covered with these tests. Results only for cylinder 1 are shown in detail for a more concise and clear representation.

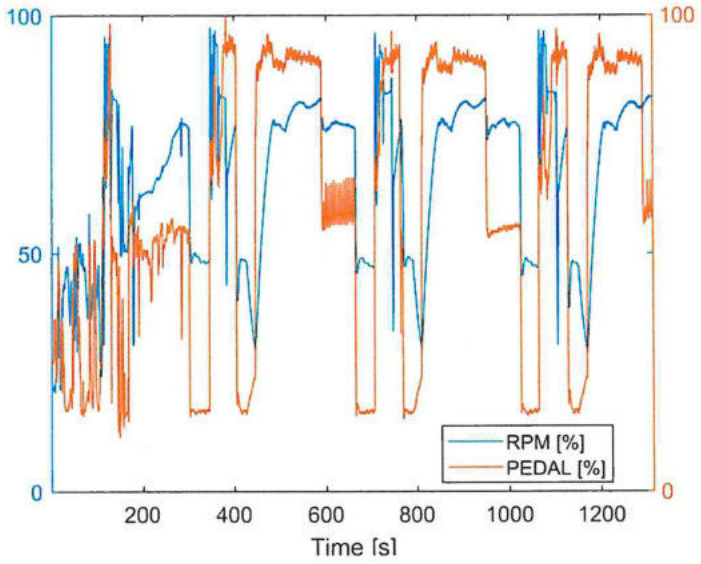


**Figure 18.** Normalized engine speed and pedal profiles related to results presented below.

During the tests, the in-cylinder pressure curves and combustion indexes measured by the indicating system have been recorded to verify the accuracy of modeled values and the robustness of the control strategy. On one hand, measured MFB50, Pmax, cyclic MAPO and ΔSA determined by the controller are shown in Figure 19. On the other hand, even the calculated indexes are reported (i.e., instantaneous Pmax, target MAPO98, target Pmax, target MFB50 and damage speed values). Rather than the MAPO threshold of piston damage model, the target MAPO98 is reported because, as described above, these two indexes are equivalent (they are two different values of the same MAPO PDF) and, at the same time, the instantaneous MAPO threshold would provide the same indication of the instantaneous damage speed (already shown in the last graph of Figures 19 and 20). All the quantities reported in Figures 19 and 20 are normalized with respect to the maximum value of y-scale, which is chosen to include all the recorded values, and the MAPO graph is zoomed to optimize the data visualization. Instead, the values of ΔSA are reported as °CA. The shown MFB50 and MAPO are the measured ones to demonstrate the accuracy of the control strategy. As anticipated above, the MAPO98 shown in Figure 19 is calculated by the indicating system with a buffer of 200 cyclic values. However, such value has not a role in the management of piston damage speed. It is just evaluated to be compared with the target MAPO98 calculated by the control algorithm. In the same way, mean MFB50 is calculated by the indicating system and it is not an index included in the controller scheme. This means that there is not any kind of filter in the controller calculation chain to avoid the introduction of a delay with respect to the current combustion indexes. The target MFB50 is defined as the value that determines a given damage speed value, saturated at the maximum combustion efficiency value (MBT). Consequently, the MBT value is the lowest MFB50 targeted by the controller. Of course, the actuated SA is generally higher than the calibrated value (as observable in the third plot of Figure 19 that reports the ΔSA) and the engine operating field for which the MBT can be reached by the controller is wider than that

resulting from the standard calibration. This is due to the higher MAPO that is considered admissible (especially beyond a certain value of STAM). The most important consequence of the application of the proposed controller is a significant increase in the combustion efficiency that can be spent as a torque increase or a fuel consumption reduction. When the combustion phase value given by the conversion of the target damage speed is lower than the MBT value, the resulting target saturates to the calibrated maximum combustion efficiency value. For this reason, Pmax and MAPO98 reach the corresponding target values only when target MFB50 is higher (i.e., more retarded) than the MBT, and such cases identify also the knock-limited operating conditions. Indeed, during such portions of the test, the measured Pmax and MAPO98 are very close to the target, allowing to achieve the damage speed target, as observable in the related graph. Indeed, despite the high variability of MAPO98, the actuated SA achieves a value of such an index that oscillates around the target value. The MAPO values reported in the last graph of Figure 19 show a low variability. This is because a portion of the highest values is covered by the MAPO98 line, but also because such values are approximated by a log-normal distribution. However, the error introduced by such approximation is low and acceptable as demonstrated by the authors in [24].

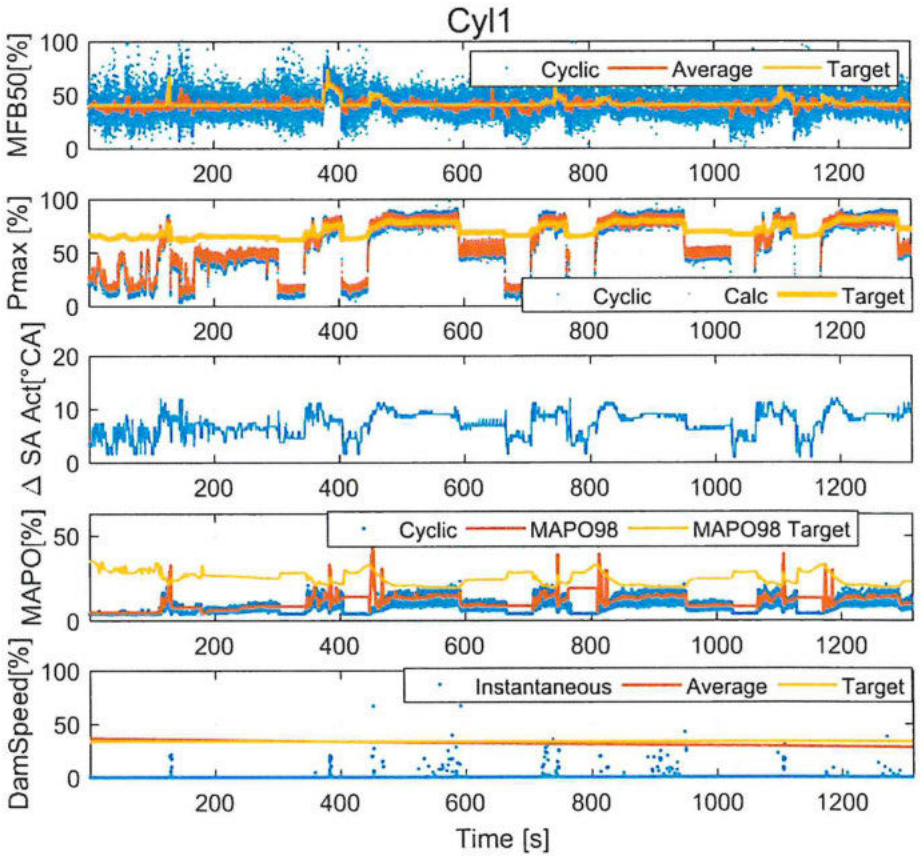


**Figure 19.** The target and the experimental values of MFB50, Pmax, MAPO, and the calculated damage speed for the cylinder 1. The second graph from the top also includes the calculated Pmax.

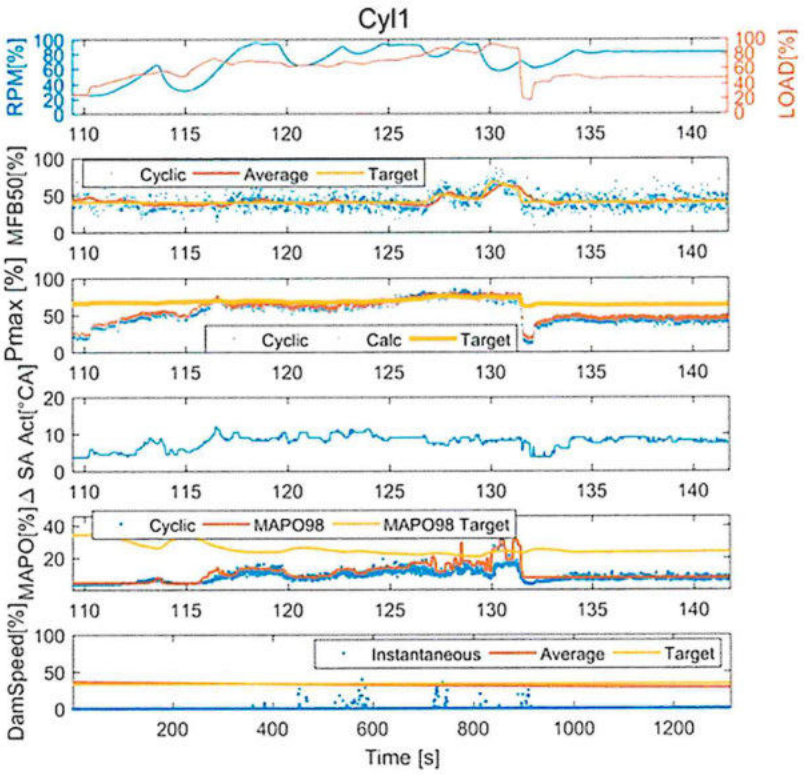


**Figure 20.** Zoom of Figure 19 between the seconds 110 and 140.

It is important to mention that the average damage speed is close to target value already at the beginning of the test and this is because the engine speed and pedal profiles shown in Figure 18 are reproduced several times in a row. In this way, the controller can reach the target damage speed value. The average damage speed shown in the last graph of Figure 19 is calculated as the cumulative damage (evaluated in bars) divided by the whole engine life (evaluated in seconds), and for this reason, it varies slowly. Even if the controller manages the instantaneous damage speed, the mean value evaluated in such a way is the most meaningful index because it represents the average damage speed on the entire engine life and the most proper value to estimate the cumulative piston damage at the end of the test period. In other words, the average damage speed calculated in this way is the index used to further validate the robustness of the piston damage model at the end of the test period. Indeed, it is directly used to estimate the resulting cumulative damage that is compared with the experimental one. At the same time, it is important to mention that the average damage speed does not have a role in the control strategy, which uses only its instantaneous value. This result demonstrates that the model-based, open-loop chain dynamically estimates the combustion indexes and converts the target damage speed into the corresponding combustion phase that achieves a desired piston surface erosion. The reliability of all the described models is therefore confirmed.

Figure 20 shows a zoom of Figure 19 between seconds 110 and 140. The first plot reports the engine speed and load in such time window (they are the corresponding values taken from Figure 18) and their trends are characterized by variations that cover the entire engine operating field. Results demonstrate the controller can keep combustion indexes close to the target values, even under rapid transient conditions. Only the moving average of MFB50 provided by the indicating system shows a slight delay with respect to the instantaneous value and the target one, but this is the common result of applying a filter. Instead, cyclic MFB50 follows with high accuracy the target (as quantified by Figure 21). It can be noted that the instantaneous damage does not only depend on the cyclic MAPO value but also on the piston temperature and thus on the engine speed and Pmax. Indeed,

the piston damage can be higher than zero (but not higher than the target) even when the MAPO98 (that is not a directly controlled index) is slightly lower than the target, depending on piston temperature values. However, when the engine speed and load conditions allow reaching target Pmax, also MAPO98 goes close to the corresponding target value. In some cases, the instantaneous damage speed exceeds the threshold, but, as it is clearly visible in the last graph of Figure 20, such exceedance is limited and always acceptable. Even if in the Part II a PI controller is introduced in the control strategy, its actions are very limited (the calculated ΔSA is always lower than 2°CA), and they react only when the instantaneous damage speed exceeds a safety threshold. At the same time, the authors can confirm that it would be inactive during the test shown in Figures 19 and 20, due to the damage speed values that remain always under the mentioned safety threshold. Hence, Figure 20 demonstrates the accuracy of the complete open-loop controller even under transient conditions.

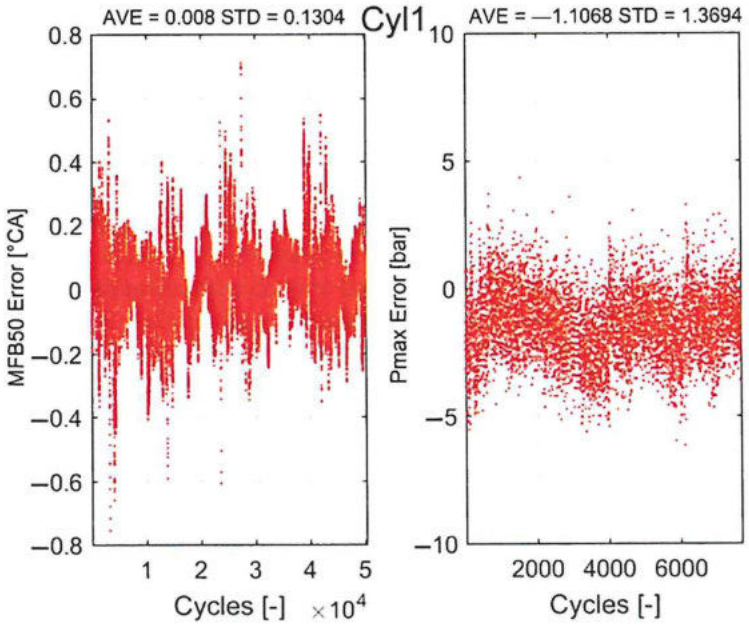


**Figure 21.** Error between the target and the experimental MFB50 and Pmax indexes, for the cylinder 1. The mean value (AVE) and the standard deviation (STD) are indicated in the title of each graph.

The calculated cyclic Pmax is often overlaid to the experimental one and this result confirms the accuracy and the robustness of the proposed analytical models that calculate the MFB50 and the maximum in-cylinder pressure. It is possible to state that the analytical MFB50 and Pmax models are extremely accurate, and they introduce negligible errors. However, a quantitative evaluation of the model accuracy is provided in Figure 21. Indeed, Figure 21 shows the percentage error between the MFB50 and Pmax, and the corresponding target values. The mean value and the standard deviation of the error are even reported. The proper way to calculate error between the target and the experimental Pmax is excluding all the engine cycles in which target MFB50 is saturated to the MBT because the target Pmax cannot be achieved. On the contrary, since the objective of this work is that to develop a combustion controller that manages the combustion phase on the entire engine operating field, the error between the MFB50 and the corresponding target value is evaluated for the whole test. For such indexes, the error is mainly within the range +−0.6 °CA and +−5 bar, respectively. These values, together with the achievement of the damage speed target, can be considered as a further confirmation of the controller accuracy and robustness.

## 5. Conclusions and Future Works

In this work, a novel model-based combustion control system is described. The proposed algorithm completely redefines the traditional knock control approaches, especially for applications in which feedback is not required, providing a solution to efficiently integrate the knock intensity management with the combustion phase control. This is possible by converting the target knock intensity values into the corresponding target MFB50, and this is realized through the implementation of a chain of models that describe the trends of main combustion indexes in a very accurate and simple way. Target knock intensity is defined as a piston erosion level, that represents the effective and tangible consequence of knocking combustion, and it is controlled through an open-loop chain that guarantees the expected behavior even under fast transient conditions. The models are developed for a designed and calibrated 8-cylinder engine. Indeed, the final controller is implemented in an RCP system that communicates the calculated spark timing corrections via CAN to the ECU, that applies such corrections to the mapped SA, for any given operating condition.

At first, a description of the main models presented in previous works of the authors is reported, deepening the latest updates and the modifications carried out for their implementation in the controller. The development and the calibration of the piston damage model is presented, underlining the novel improvements and the methodology applied for the conversion of target damage speed into a target MAPO percentile. The analytical knock model is calibrated for the 8-cylinder engine used for this work and it is reversed to convert the target MAPO percentile into the corresponding Pmax value. The main benefits of the simple analytical formulation are thus shown. The analytical Pmax and MFB50 models are briefly retrieved and the implementation of the ΔSA-MFB50 parabolic function is discussed. The model-based open-loop chain converts the target piston damage speed into a target combustion phase, saturated to the MBT.

The validation is performed by reproducing at the engine bench the speed and load profiles logged during real, on-track vehicle maneuvers, to test the combustion controller under fast transient conditions.

The results demonstrate both the robustness of the complete open-loop chain and the high accuracy of the combustion models, returning very small errors in estimating main combustion indexes. However, as already mentioned, it is important to highlight the described pure open-loop controller cannot estimate accurate combustion indexes when events that are not considered by the models occur, such as the engine or the exhaust system aging. However, the presented models can be further developed to introduce the dependency to such kinds of events. Of course, the availability of a measurement of the MFB50 and MAPO can prevent undesirable events. Nevertheless, the results achieved with the open-loop controller are valuable (error of +−0.6 °CA on MFB50 and +−5 bar on Pmax) and the presented tests demonstrate the general validity of the proposed approach. More generally, a SA higher than the mapped value is applied by the controller and a significant combustion efficiency increase is achieved.

Such controller is concretely used for special applications, and it will be further developed with an exhaust gas temperature model to manage even the lambda target and then it will be implemented in a prototyping ECU. Indeed, modern ECUs are characterized by high computational power and their main limitation is related to the number of analog and digital channels, rather than the CPU power. Even if the computational effort strongly depends on the type of RT machine used to perform the tests, the authors confirm that the proposed controller is suitable for the implementation in a production ECU.

In the second paper (Part 2) focused on this topic, the open-loop combustion controller is further developed by introducing a PI controller and model-based adaptive strategies that automatically determine the fuel RON value and update the analytical relationship between the ΔSA and the MFB50. Of course, such adaptive strategies need the measurement of the knock intensity and of the combustion phase, but this can be considered as a viable solution also for on-board applications, due to the availability of commercial systems that can estimate such indexes. Such development is needed when the controller has to be

applied to production systems. The resulting controller will be directly deployed on a prototyping ECU and validated at the engine test bench.

**Author Contributions:** Formal analysis, M.C. and N.S.; Supervision, N.C., N.R., J.M., E.C. and V.R.; Writing—original draft, A.B. All authors have read and agreed to the published version of the manuscript.

**Funding:** This work was supported by 1 research grants founded by the Department of Industrial Engineering of the University of Bologna (grant number 2616) and the collaboration with Ferrari S.p.a. The external funding is indicated in the Acknowledgments section.

**Acknowledgments:** The authors gratefully acknowledge financial support from "Fondi europei della Regione Emilia-Romagna", within program POR FSE 2014–2020 in the framework of the "Accordo Regionale di insediamento e sviluppo delle imprese—progetto STEP".

**Conflicts of Interest:** The authors declare no conflict of interest.

## Abbreviations

| | |
|---|---|
| BMEP | Brake Mean Effective Pressure |
| CAN | Controller Area Network |
| ECU | Engine Control Unit |
| FEM | Finite Element Method |
| GDI | Gasoline Direct Injection |
| HB | Brinell-Hardness |
| HTT | Hardness-Time-Temperature curves |
| IMEP | Indicating Mean Effective Pressure |
| ION | Ionization Current |
| MAPO | Maximum Amplitude of Pressure Oscillation |
| MAPO98 | 98th percentile of MAPO |
| MAPO99.5 | 99.5th percentile of MAPO |
| MBT | Maximum Brake Torque |
| MFB50 | The 50%-of-Mass-of-Fuel-Burned |
| PDF | Probability Density Function |
| PF | Probability Function |
| PID | Proportional Integral Derivative controller |
| Pmax | Maximum in-cylinder pressure |
| Pmax90 | 90th percentile of Pmax |
| RCP | Rapid Control Prototyping |
| RON | Research Octane Number |
| RT | Real-Time |
| RzD | Roughness Depth index |
| SA | Spark Advance |
| STAM | Stoichiometric Trapped Air Mass |
| TAM | Trapped Air Mass |
| TC | Turbo-Charged |
| VVT | Variable Valve Timing |

## References

1. Wang, Z.; Liu, H.; Reitz, R. Knocking combustion in spark-ignition engines. *Prog. Energy Combust. Sci.* **2017**, *61*, 78–112. [CrossRef]
2. Corti, E.; Forte, C. *Statistical Analysis of Indicating Parameters for Knock Detection Purposes*; SAE Technical Paper; SAE: Warrendale, PA, USA, 2009. [CrossRef]
3. Spelina, J.; Peyton Jones, J.; Frey, J. Recent advances in knock analysis, simulation, and control. *SAE Int. J. Engines* **2014**, *7*, 947–955. [CrossRef]
4. Gao, J.; Yao, A.; Feng, L.; Xu, H.; Yao, C. *Experimental Investigation on the Failures of Engine Piston Subjected to Severe Knock*; SAE Technical Paper; SAE: Warrendale, PA, USA, 2019. [CrossRef]
5. Samimy, B.; Rizzoni, G.; Leisenring, K. *Improved Knock Detection by Advanced Signal Processing*; SAE Technical Paper; SAE: Warrendale, PA, USA, 1995. [CrossRef]

6. De Cesare, M.; Ravaglioli, V.; Carra, F.; Stola, F. *Review of Combustion Indexes Remote Sensing Applied to Different Combustion Types*; SAE Technical Paper; SAE: Warrendale, PA, USA, 2019. [CrossRef]
7. Moro, D.; Cavina, N.; Ponti, F. In-cylinder pressure reconstruction based on instantaneous engine speed signal. *ASME J. Eng. Gas Turbines Power* **2002**, *124*, 220–225. [CrossRef]
8. Romani, L.; Bianchini, A.; Vichi, G.; Bellissima, A.; Ferrara, G. Experimental assessment of a methodology for the indirect in-cylinder pressure evaluation in four-stroke internal combustion engines. *Energies* **2018**, *11*, 1982. [CrossRef]
9. Shimasaki, Y.; Kobayashi, M.; Sakamoto, H.; Ueno, M.; Hasegawa, M.; Yamaguchi, S.; Suzuki, T. *Study on Engine Management System Using In-cylinder Pressure Sensor Integrated with Spark Plug*; SAE Technical Paper; SAE: Warrendale, PA, USA, 2004. [CrossRef]
10. Franke, A.; Reinmann, R.; Larsson, A. *The Role of the Electrodes for the Ionization Sensor Signal*; SAE Technical Paper; SAE: Warrendale, PA, USA, 2003. [CrossRef]
11. Panousakis, D.; Gazis, A.; Patterson, J.; Chen, R. *Analysis of SI Combustion Diagnostics Methods Using Ion-Current Sensing Techniques*; SAE Technical Paper; SAE: Warrendale, PA, USA, 2006. [CrossRef]
12. **Cavina, N.; Poggio, L.; Sartoni, G. Misfire and partial burn detection based on ion current measurement.** *SAE Int. J. Engines* **2011**, *4*, 2451–2460. [CrossRef]
13. Tong, S.; Li, H.; Yang, Z.; Deng, J.; Hu, Z.; Li, L. *Cycle Resolved Combustion and Pre-Ignition Diagnostic Employing Ion Current in a PFI Boosted SI Engine*; SAE Technical Paper; SAE: Warrendale, PA, USA, 2015. [CrossRef]
14. Peyton Jones, J.; Muske, K.; Frey, J.; Scholl, D. *A Stochastic Knock Control Algorithm*; SAE Technical Paper; SAE: Warrendale, PA, USA, 2009. [CrossRef]
15. Spelina, J.M.; Peyton Jones, J.C.; Frey, J. Characterization of knock intensity distributions, Part I: Statistical independence and scalar measures. *Proc. Inst. Mech. Eng. Part D J. Auto Eng.* **2017**, 117–128. [CrossRef]
16. Spelina, J.M.; Peyton Jones, J.C.; Frey, J. Characterization of knock intensity distributions, Part II: Parametric models. *Proc. Inst. Mech. Eng. Part D J. Auto Eng.* **2013**, *227*, 1650–1660. [CrossRef]
17. Peyton Jones, J.C.; Spelina, J.M.; Frey, J. Likelihood-based Control of Engine Knock. *IEEE Trans. on Control Sys. Tech.* **2013**, *1*. [CrossRef]
18. Thomasson, A.; Shi, H.; Lindell, T.; Eriksson, L.; Shen, T.; Jones, J.C.P. Tuning and Experimental Evaluation of a Likelihood-Based Engine Knock Controller. In Proceedings of the 2013 IEEE 52nd Conference on Decision & Control, Firenze, Italy, 10–13 December 2013. [CrossRef]
19. Spelina, J.M.; Peyton Jones, J.C.; Frey, J. Stochastic simulation and analysis of a classical knock controller. *Int. J. Engine Res.* **2014**, *16*, 461–473. [CrossRef]
20. Frey, J.; Peyton Jones, J.C. Stochastic simulation of a cumsum knock controller. *IFAC-PapersOnLine* **2016**, *49–11*, 210–216. [CrossRef]
21. Shayestehmanesh, S.; Peyton Jones, J.; Frey, J. *Stochastic Characteristics of Knock and IMEP*; SAE Technical Paper; SAE: Warrendale, PA, USA, 2018. [CrossRef]
22. Peyton Jones, J.; Frey, J. performance assessment of knock control systems subject to disturbances. *SAE Int. J. Engines* **2021**, *14*. [CrossRef]
23. Cavina, N.; Rojo, N.; Ceschini, L.; Balducci, E.; Poggio, L.; Calogero, L.; Cevolani, R. *Investigation of Knock Damage Mechanisms on a GDI TC Engine*; SAE Technical Paper; SAE: Warrendale, PA, USA, 2017. [CrossRef]
24. Cavina, N.; Brusa, A.; Rojo, N.; Corti, E. *Statistical Analysis of Knock Intensity Probability Distribution and Development of 0-D Predictive Knock Model for a SI TC Engine*; SAE Technical Paper; SAE: Warrendale, PA, USA, 2018. [CrossRef]
25. Brusa, A.; Cavina, N.; Rojo, N.; Cucchi, M.; Silvestri, N. *Development and Validation of a Control-Oriented Analytic Engine Simulator*; SAE Technical Paper; SAE: Warrendale, PA, USA, 2019. [CrossRef]
26. Abgrall, R.; Shu, C.-S. *Handbook of Numerical Methods for Hyperbolic Problems*; Springer: Berlin/Heidelberg, Germany, 2017; ISBN 9780444639103.
27. Ceschini, L.; Morri, A.; Balducci, E.; Cavina, N.; Rojo, N.; Calogero, L.; Poggio, L. Experimental observations of engine piston damage induced by knocking combustion. *Mater. Des.* **2017**, *114*, 312–325. [CrossRef]
28. Balducci, E.; Ceschini, L.; Rojo, N.; Cavina, N.; Cevolani, R.; Barichello, M. Knock induced erosion on Al pistons: Examination of damage morphology and its causes. *Eng. Fail. Anal.* **2018**, *92*, 12–31. [CrossRef]
29. Ceschini, L.; Morri, A.; Morri, A.; di Sabatino, M. Effect of thermal exposure on the residual hardness and tensile properties of the EN AW-2618A piston alloy. *Mater. Sci. Eng. A* **2015**, *639*, 288–297. [CrossRef]
30. Balducci, E.; Ceschini, L.; Morri, A.; Morri, A.; di Sabatino, M.; Arnberg, L.; Li, Y. High temperature behavior of the EN AW-2618A **piston alloy containing 0.12wt% Zr: Influence of heat treatment.** *Mater. Today Proc.* **2015**, *2*, 5037–5044. [CrossRef]
31. DIN 4768. *Determination of Values of Surface Roughness Parameters Ra, Rz, And Rmax Using Electrical Contact (Stylus) Instruments Concepts and Measuring Conditions*, 1990th ed.; Deutsches Institut für Normung: Berlin, Germany, 1990.
32. Cantore, G.; Giacopini, M.; Rosi, R.; Strozzi, A.; Pelloni, P.; Forte, C.; Achilluzzi, M.; Bianchi, G.M.; Ceschini, L.; Morri, A. Validation of a Combined CFD/FEM Methodology for the Evaluation of Thermal Load Acting on Aluminum Alloy Pistons through Hardness Measurements in Internal Combustion Engines. In *Metallurgical Science and Technology*; Public Knowledge Project: Vancouver, BC, Canada, 2011.
33. Mahle, G.M.B.H. *Piston and Engine Testing*; Springer: Berlin/Heidelberg, Germany, 2012.
34. Cesari, F. *Calcolo Matriciale delle Strutture 2*; Pitagora Editrice Bologna: Bologna, Italy, 1997.

35. Cesari, F. *Meccanica delle Strutture. Metodo degli Elementi Finiti. 120 Problemi Risolti*; Pitagora Editrice Bologna: Bologna, Italy, 2011.
36. Timoshenko, S.P. *Theory of Elasticity*, 3rd ed.; McGraw-Hill: New York, NY, USA, 1970.
37. Matlab Documentation. The MathWorks. 2021. Available online: https://www.mathworks.com/ (accessed on 20 April 2021).
38. Ghandhi, J.; Kim, K. *A Statistical Description of Knock Intensity and Its Prediction*; SAE Technical Paper; SAE: Warrendale, PA, USA, 2017. [CrossRef]